https://doi.org/10.5194/egusphere-2025-5502
Preprint. Discussion started: 20 November 2025

Understanding divergent Brown Carbon Photobleaching Rates from Molecular Perspective

Yanting Qiu[1], Tao Qiu[2], Yuechen Liu[3], Yu Gu[2], Ruiqi Man[1], Dapeng Liang[2], Taomou Zong[1], Zhijun Wu[1,4,], Min Hu[1]*

1 State Key Laboratory of Regional Environment and Sustainability, College of Environmental Sciences and Engineering, Peking University, Beijing 100871, China

2 Key Lab of Groundwater Resources and Environment of the Ministry of Education, College of New Energy and Environment, Jilin University, Changchun 130012, China

3 National Institute of Metrology, Beijing 100029, China

4 Collaborative Innovation Center of Atmospheric Environment and Equipment Technology, Nanjing University of Information Science and Technology, 210044, Nanjing, China

*Correspondence Author:

Zhijun Wu (zhijunwu@pku.edu.cn)

KEYWORDS. brown carbon; photochemical aging; brown carbon photobleaching; biomass burning aerosol; non-target analysis

https://doi.org/10.5194/egusphere-2025-5502
Preprint. Discussion started: 20 November 2025

ABSTRACT

The global radiative effect of brown carbon (BrC) remains highly uncertain. BrC's photobleaching, which significantly alerts its radiative effect, has been still poorly constrained. This study investigates photobleaching rates of laboratory-synthesized secondary BrC (aq-BrC), biomass burning-derived BrC (b-BrC), and ambient $PM_{2.5}$-derived BrC (p-BrC). Our results reveal a source dependence in BrC photobleaching rates. The highest photobleaching rate constant (k_{BrC}) is observed for aq-BrC (1.13 ± 0.08 h^{-1}), followed by p-BrC (0.12 ± 0.02 h^{-1}) and b-BrC (0.05 ± 0.01 h^{-1}), indicating the stable light-absorption capacity of b-BrC in the atmosphere. The OH oxidation of imidazole-2-carboxaldehyde (2-IC) and methylglyoxal oligomers, nitrophenols (including phenols), and lignin derivatives governs the photobleaching of aq-BrC, p-BrC, and b-BrC, respectively. The high k_{BrC} of aq-BrC is attributed to the high reactivity of the chain structures in 2-IC and methylglyoxal oligomers. In contrast, the highly conjugated structures of lignin derivatives in b-BrC impart stability against OH oxidation, resulting in a low k_{BrC}. Our findings reveal the significant differences in the photobleaching behavior of BrC originated from different sources, underscoring the crucial need to account for source differences in assessments of BrC's global radiative forcing effect.

https://doi.org/10.5194/egusphere-2025-5502
Preprint. Discussion started: 20 November 2025

1. Introduction

Brown carbon (BrC) is a significant contributor to atmospheric warming (Saleh, 2020; Chung et al., 2012; Brown et al., 2021) and Earth's radiative budget (Bond, 2001; Kirchstetter et al., 2004; Wang et al., 2018; Wang et al., 2022) due to its ultraviolet-visible (UV-Vis) light absorption. The BrC's direct radiative effect (DRE), accounting for 20%–40% of total DRE caused by light-absorbing carbonaceous aerosols (Heald et al., 2014; Jo et al., 2016; Saleh et al., 2015; Wang et al., 2018; Wang et al., 2014), remains highly uncertainty. BrC with global average DRE values varying from +0.03 to +0.57 W/m^2 is considered as the least understood warming agents in the atmosphere (Zhang et al., 2020; Zeng et al., 2020; Corr et al., 2012).

BrC comprises abundant chemically reactive species that react readily with atmospheric reactive gases and radicals (Aiona et al., 2017; Fleming et al., 2020; Hems et al., 2021; Liu et al., 2020), modifying its light-absorption properties. Both laboratory experiments (Borduas-Dedekind et al., 2019; Fleming et al., 2019; Hems and Abbatt, 2018; Hems et al., 2020; Schnitzler and Abbatt, 2018; Schnitzler et al., 2022) and field campaigns (Dasari et al., 2019; Qiu et al., 2024; Wang et al., 2014; Xu et al., 2024; Zeng et al., 2020) consistently found that BrC's photochemical aging process reduced its mass absorption coefficient (MAC), which is also known as photobleaching. In current models, the evaluation of BrC photobleaching on its radiative forcing mainly depends on the temporal evolution of BrC's light-absorption capacity (Schnitzler et al., 2022; Wang et al., 2018; Xu et al., 2024), i.e., the photobleaching rate, which is substantial variability across different laboratory experiments and field observations. Notably, BrC generated from aqueous-phase reactions often exhibits negligible absorbance in the UV-Vis range after less than 2 hours of radiation (Aiona et al., 2017). Field observations reveal that atmospheric BrC undergoes a MAC reduction exceeding 60% after 1 day of sunlight exposure (Müller et al., 2023; Qiu et al., 2024). In comparison, over the same 1 day of solar radiation, the reduction in BrC derived from biomass burning is much lower than atmospheric BrC (Fan et al., 2019; Fleming et al., 2020; Müller et al., 2023; Wong et al., 2019). Overall, accurately determining BrC's photobleaching rate is paramount for quantifying the impact of BrC photobleaching on its radiative forcing effect in models.

Furthermore, BrC's chemical composition fundamentally governs its photochemical reactivity (Hems et al., 2021; Hems and Abbatt, 2018; Dalton and Nizkorodov, 2021; Liu et al., 2025), thereby modulating its photobleaching rate. However, the relationship between changes in BrC's molecular composition and light absorption properties during the photobleaching is still poorly constrained. This knowledge gap leads to significant uncertainty in evaluating the evolution of BrC's light absorption capacity during atmospheric transportation. For instance, BrC emitted from biomass burning has been observed to retain strong absorption after several days of transport to the Arctic (Yue et al., 2022). In contrast, model simulations estimate BrC is nearly complete photobleaching over this timescale (Wang et al., 2018; Xu et al., 2024), which contradicts the observational evidence. Elucidating the linkage between BrC molecular composition and photobleaching rates would improve the accuracy of global-scale assessments of BrC's dynamic light absorption properties during long-range transport.

In this work, we performed photochemical aging experiments on three types of BrC, including synthesised by aqueous phase reaction (referred to "aq-BrC"), and extracted from ambient (referred to "p-BrC") and biomass

https://doi.org/10.5194/egusphere-2025-5502
Preprint. Discussion started: 20 November 2025

burning (referred to "b-BrC") $PM_{2.5}$ samples. We found that the photobleaching rates of BrC from different sources vary significantly. High-resolution mass spectrometry (HRMS) analysis was adopted to provide molecular-level understanding of this source-dependent BrC photobleaching rate. In addition, OH oxidation was determined as the dominate pathway of BrC photobleaching. These findings highlight the importance of considering differences in BrC sources when assessing its global radiative forcing effect.

2. Methodology

2.1 Preparation of BrC

Methylglyoxal (MG, 40 wt%, Merck) and ammonium sulfate (AS, 98%, Alaadin) solutions (1 mol/L) was mixed in darkness at room temperature for 2 h (pH 3.7–4.2) (Yang et al., 2024) to generate aq-BrC. Residual MG/AS were removed by solid-phase extraction (SPE) (Lin et al., 2010; Wang et al., 2017). The eluent was dried under gentle stream of ultrapure N_2 (>99.99%) and reconstituted in ultrapure water (18.2 MΩ·cm).

$PM_{2.5}$ samples emitted from corn straw combustion in household stoves was collected on quartz fiber filters (25 × 20 cm, Whatman) using a high-volume sampler (TH-1000H, Wuhan Tianhong; 1.05 m^3/min). Figure S1 shows a schematic of sample collection process of biomass burning $PM_{2.5}$ samples, and Table S1 summarizes the concentrations of organic carbon (OC), element carbon (EC), the concentration of total organic carbon (TOC) of each sample. This approach closely represents real-world biomass burning emissions (Chen et al., 2019; Shan et al., 2017). For each sample, background aerosols were collected for 1 hour both before to and after the sampling period.

Atmospheric $PM_{2.5}$ samples were collected at Peking University Changping Campus (40°8′N, 116°6′E) from 15 December 2020 to 15 January 2021 using a high-volume sampler. The sampling period of each sample was 23 hours. Gaseous pollutants, $PM_{2.5}$ mass concentrations, non-refractory submicron particles (NR-PM_1) chemical composition, and meteorology were monitored (Figure S2; details in Table S2).

For those $PM_{2.5}$ samples, twenty 1.5-cm^2 filter sections were ultrasonically extracted in LC-MS grade methanol (Merck Inc.) for twice (20 min) to extract p-BrC and b-BrC. Extracts were dried gentle stream of ultrapure N_2 (>99.99%) and redissolved in ultrapure water.

2.2 Laboratory aqueous-phase photochemical aging setup

Photochemical aging experiments were conducted in a temperature-controlled (20 ± 0.1 °C) chamber, equipped with 20 UV bulbs (40 W; λ_{max}= 370 nm). The TOC of all BrC solutions were adjusted to 50 mgC/L. BrC solutions were irradiated in quartz bottles (10 mL) with added H_2O_2 (30 wt%, Alaadin) to generate OH radicals. Steady-state OH concentrations ($[OH]_{ss}$) were quantified via pseudo-first-order decay of benzoic acid (methods detailed in Text S1) (Hems and Abbatt, 2018). The average $[OH]_{ss}$ was (3.17 ± 0.47) × 10^{-14} mol/L, slightly below typical cloud water maxima. Laboratory irradiation times were converted to equivalent solar durations using a spectral flux density ratio (scaling factor: 3.86) (Qiu et al., 2024). Samples were collected at 0, 2, 4, 8, and 16 hours of equivalent solar radiation.

https://doi.org/10.5194/egusphere-2025-5502
Preprint. Discussion started: 20 November 2025

Furthermore, a series of control experiments were performed under H_2O_2 free and dark conditions. In both cases, the same BrC solutions (50 mgC/L TOC) were used for different types of BrC. The former consisted of 16 hours of radiation in the absence of H_2O_2. The dark experiments involved storing the solutions in complete darkness for an identical period (16 hours) to account for any non-photochemical changes.

These experiments were configured to delineate the contributions of different pathways to BrC photobleaching. The H_2O_2 added photochemical aging experiments elucidates the synergistic effect of OH oxidation, direct BrC photolysis, and other light-independent reactions occur in dark conditions. The H_2O_2 free experiments considered the sole contribution of the direct photolytic pathway. In addition, the dark control experiments served to investigate any potential influence of chemical reactions in dark conditions on the BrC's light-absorption capacity.

2.3 Light-absorption properties and molecular composition analysis of BrC

UV-Vis absorption spectra (250–700 nm) were recorded using a spectrophotometer (UV-1780, Shimadzu Inc.). MAC normalized absorption to TOC concentrations. In eq.(1), $A_{10}^{abs}(\lambda)$, b, and c denotes the measured base-10 absorbance, optical path length (1 cm), and measured TOC, respectively.

$$\mathrm{MAC}(\lambda) = \frac{A_{10}^{abs}(\lambda) \times \ln(10)}{b \times c} \qquad (1)$$

BrC's molecular composition was analyzed via HRMS (Orbitrap Fusion™ Tribrid™, Thermo Scientific) with electrospray ionization (ESI) in negative mode (ESI(-); *m/z* 70–700). Samples were directly injected into HRMS at a flow rate of 10 μL/min. Triplicate analyses ensured reproducibility, with only peaks detected in all replicates retained for assignment. Molecular formulas ($C_xH_yO_zN_wS_n$; x = 1–90, y = 1–200, z = 0–20, w = 0–3, n = 0–1) were assigned with *m/z* error lower than ± 0.005 Da. The H/C, O/C, N/C, and S/C atom ratios for each assigned formula were constrained to 0.3–3.0, 0–3.0, 0–0.5, and 0–2.0, respectively(Wang et al., 2017). Signal-intensity-weighted average elemental compositions (eq.(2)), O/C atom ratios, and N/C atom ratios (eq.(3)) were calculated as:

$$\mathrm{Y} = \frac{\sum_i x_i Y_i}{\sum_i x_i}, \text{ where Y = C, H, O, N, and S} \qquad (2)$$

$$\mathrm{Y/Z} = \frac{\sum_i x_i Y_i}{\sum_i x_i Z_i}, \text{ where Y/Z = O/C or N/C} \qquad (3)$$

where x_i in eqs. (2) and (3) indicated the signal-intensity-weighted factor.

3. Results and Discussion

3.1 BrC Photobleaching rates

Given that BrC's light-absorption properties at shorter wavelengths are a better indicator of its photobleaching kinetics (Aiona et al., 2017), we focused our analysis on the variation in the MAC at 300 nm

https://doi.org/10.5194/egusphere-2025-5502
Preprint. Discussion started: 20 November 2025

(MAC_{300}). Figure 1(a) shows the decay of MAC_{300} for different BrC types, plotted as the natural logarithm of the ratio ($\ln(MAC_{300,t}/MAC_{300,0})$) versus irradiation hours. Here, $MAC_{300,t}$ and $MAC_{300,0}$ denote the MAC_{300} after t hours of irradiation and its initial value, respectively. The observed linear decay demonstrates that BrC undergoes photobleaching regardless of its source. The aq-BrC has been almost completely bleached in the initial 2 hours. The MAC_{300} decreased by 77.2% after 16 hours of radiation. In comparison, for b-BrC, the MAC_{300} only decreased by 56.1%. Even after extending to 32 hours of radiation, b-BrC still kept strong light-absorption capacity (see Figure S3). The differences in the variation in MAC_{300} for different types of BrC demonstrate that aq-BrC undergoes rapid photobleaching in the presence of solar radiation, while b-BrC exhibits stable light-absorption capacity during photobleaching.

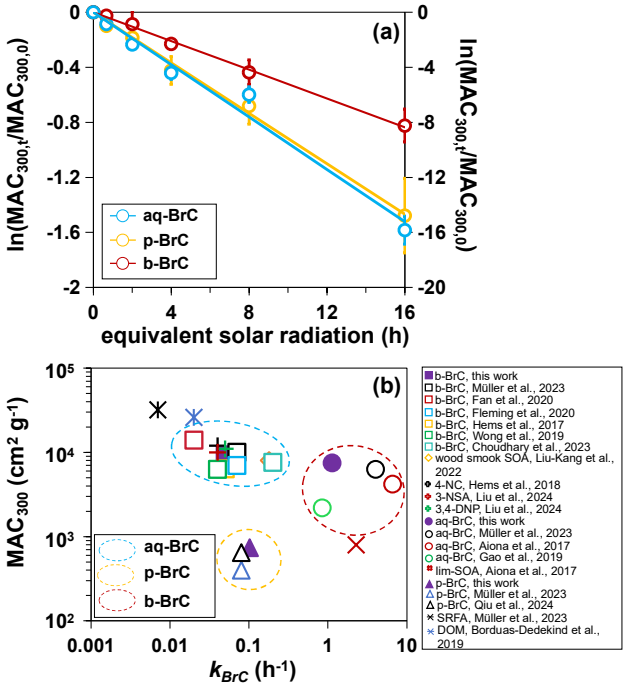

Figure 1 (a) Variations in the $\ln(MAC_{300,t}/MAC_{300,0})$ of aq-BrC (blue plots, right axis), p-BrC (yellow plots, left axis), and b-BrC (red plots, left axis) as a function of radiation hours. Blue, yellow, and red lines indicate fitted k_{BrC} of aq-BrC, p-BrC, and b-BrC. Error bars represent one standard deviation of datapoints derive from three (aq-BrC and b-BrC) or five (p-BrC) parallel experiments. (b) The relationship between MAC_{300} and calculated k_{BrC} of different types of BrC in this work and other studies. 4-NC, 3-NSA, 3,4-DNP, SRFA, and DOM represents 4-nitrocateol, 3-mitrosalicylic acid, 3,4-dinitrophenol, Suwannee River fulvic acid standard, and dissolved organic matters, respectively. Blue, yellow, and red circles marked aq-BrC (including BrC generated via aldehyde-amine condensation reactions), p-BrC, and b-BrC (including representative compounds emitted from biomass burning). The exact MAC_{300} values are obtained from figures in corresponding literatures, and k_{BrC} are calculated based on the MAC_{300} and hours of radiation.

https://doi.org/10.5194/egusphere-2025-5502
Preprint. Discussion started: 20 November 2025

The liner decline in ln($MAC_{300,t}/MAC_{300,0}$) indicates that BrC photobleaching fitted the pseudo-first order kinetic, which was represented by the negative slope of ln($MAC_{300,t}/MAC_{300,0}$) vs. radiation hours:

$$MAC_{300,t} = MAC_{300,0} \times \exp(-k_{BrC}t) \qquad (4)$$

where k_{BrC} is the apparent photobleaching rate constant. The calculated k_{BrC} of aq-BrC, p-BrC, and b-BrC were (1.13±0.08) $hour^{-1}$, (0.12±0.02) $hour^{-1}$, and (0.05±0.01) $hour^{-1}$, respectively. Correspondingly, the lifetime of BrC (τ_{BrC}, indicated by BrC's absorption decreased to 1/e of its initial value) (Schnitzler et al., 2022) were 1.05 hours, 10.91 hours, and 19.16 hours, respectively. Longer τ_{BrC} of b-BrC indicates its absorption largely retains during atmospheric transportation process.

Figure 1(b) presents a comparison of MAC_{300} versus k_{BrC} for BrC from various sources, including data from this study and other studies (data and references in Table S3). Based on their sources, we classified aq-BrC (including BrC generated via aldehyde-amine condensation reactions), p-BrC, and b-BrC (including representative compounds emitted from biomass burning) in three different clusters. Our results are comparable to those of previous studies. The characteristic of aq-BrC is strong absorption, rapid photobleaching. This demonstrates that the light-absorption capacity of BrC generated by atmospheric aqueous phase reactions (De Haan et al., 2017) decrease rapidly in the presence of solar radiation. In stark contrast, b-BrC shows strong absorption but slow photobleaching, implying its stable strong absorption in the atmosphere. p-BrC exhibits weak absorption and slow photobleaching, which has also been observed in different urban areas, including Eastern China (Qiu et al., 2024), India (Dasari et al., 2019), Northern Europe(Müller et al., 2023), and the United States (Chen et al., 2021).

Having investigated the differences in photobleaching rates across different BrC types, we further elucidated the underlying mechanisms by assessing the contribution of each photobleaching pathway. Previous studies suggest that BrC photobleaching occurs via three different pathways, including direct photolysis, OH oxidation, and other light-independent reactions occur in dark conditions (Gao and Zhang, 2019; Liu-Kang et al., 2022; Wong et al., 2019). Choudhary et al. (2023) (Choudhary et al., 2023) have demonstrated that in the presence of H_2O_2, the k_{BrC} can be expressed as a linear sum of the pseudo first-order effective photobleaching rate constant due to OH oxidation ($k_{BrC,OH}$), BrC direct photolysis ($k_{BrC,pho}$), and other light-independent reactions occur in dark conditions ($k_{BrC,ctrl}$), see eq. (5):

$$k_{BrC} = k_{BrC,OH} + k_{BrC,pho} + k_{BrC,ctrl} \qquad (5)$$

The $k_{BrC,pho}$ and $k_{BrC,ctrl}$ are derived from the pseudo-first-order decay of MAC_{300} in H_2O_2 free experiments and dark control experiments, respectively, using the calculation approach identical to eq. (4) and the experimental procedures detailed in Section 2.2. Therefore, although $k_{BrC,OH}$ cannot be measured directly, it can be indirectly determined by calculating the difference between the k_{BrC} and the sum of $k_{BrC,pho}$ (from H_2O_2 free experiments) and $k_{BrC,ctrl}$ (from dark control experiments).

Figure 2 displays the variations in MAC_{300} in photochemical aging experiments (with H_2O_2, red line, representing the synergistic effect of OH oxidation, direct BrC photolysis, and other light-independent reactions occur in dark conditions), H_2O_2 free experiments (blue line, representing the contribution of BrC direct photolysis), and dark control experiments (black line, representing the contribution of other light-independent

https://doi.org/10.5194/egusphere-2025-5502
Preprint. Discussion started: 20 November 2025

reactions occur in dark conditions). It is noted that for dark control experiments, the x-axis denotes the time the BrC solution is kept under dark conditions. MAC_{300} variations were negligible in dark controls, rendering the calculated $k_{BrC,ctrl}$ was close to 0. For all BrC types, $k_{BrC,pho}$ was substantially lower than $k_{BrC,OH}$. Specifically, the $k_{BrC,pho}$ was (0.19±0.03) h^{-1}, (0.02±0.005) h^{-1}, and (0.01±0.004) h^{-1} for aq-BrC, p-BrC, and b-BrC, respectively. The calculated $k_{BrC,OH}$ was (0.94±0.06) h^{-1}, (0.08±0.02) h^{-1}, and (0.04±0.01) h^{-1} for aq-BrC, p-BrC, and b-BrC.

For all types of BrC, the overwhelming contribution of $k_{BrC,OH}$ (over 80% of k_{BrC}) unambiguously identifies OH oxidation as the dominant mechanism governing BrC photobleaching. Consequently, the observed differences in k_{BrC} among different types of BrC can be fundamentally attributed to the molecular-composition-dependent reactivity of BrC components toward OH radicals. Hence, understanding the underlying molecular composition that determine a BrC molecule's susceptibility to this OH oxidation.

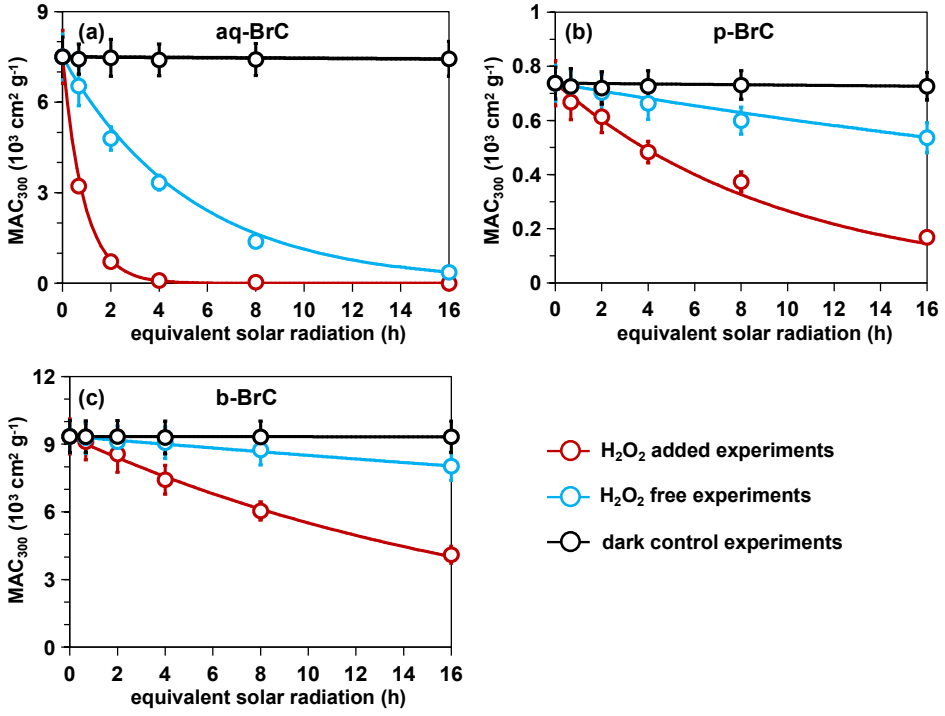

Figure 2 The variations in MAC_{300} in photochemical aging experiments (with H_2O_2, red line, representing the synergistic effect of OH oxidation, direct BrC photolysis, and other light-independent reactions occur in dark conditions), H_2O_2 free experiments (blue line, representing the variation in MAC_{300} contributed by BrC direct photolysis), and dark control experiments (black line, representing the variation in MAC_{300} contributed by other light-independent reactions occur in dark conditions) for (a) aq-BrC, (b) p-BrC, and (c) b-BrC, respectively. For dark control experiments (black line), the x-axis represents the time the BrC solution is kept in the absence of light.

https://doi.org/10.5194/egusphere-2025-5502
Preprint. Discussion started: 20 November 2025

3.2 Chemical investigation of different BrC photobleaching rates

To elucidating the differences in BrC photobleaching rates, we investigated BrC's molecular composition before and after photobleaching, which was represented by BrC's molecular composition after 16 hours of radiation.

Table 1 summarizes the signal-intensity-weighted average elemental compositions, molecular weights, O/C ratios, and N/C ratios of different types of BrC before and after 16 hours of radiation. The observed decrease in average molecular weights upon photobleaching across all BrC types, alongside an elevated O/C ratio, points to the production of more oxidized, lower-mass species. Additionally, we found the mass concentrations of low-molecular-weight organic acids (formic acid, acetic acid, and oxalic acid; see Figure S4) significantly increased with longer radiation hours, demonstrating carbon backbone fragmentation (Borduas-Dedekind et al., 2019). Figure S5 demonstrates that more products with lower C atom numbers are detected after photobleaching, further proves the carbon backbone fragmentation. Considering OH oxidation dominates BrC photobleaching, the molecular-level evolution aligns with OH-mediated degradation pathways (Hems et al., 2020; Qiu et al., 2024; Liu et al., 2025): (i) electrophilic addition to unsaturated bonds (like C=C bonds) and (ii) subsequent carbon backbone fragmentation.

In addition, the reduced N/C atom ratios (Table 1) further confirmed degradation of N-containing compounds, which are key UV-Vis absorbers contributing significantly to BrC absorption (Lin et al., 2017; Wang et al., 2019; Zeng et al., 2021; Li et al., 2025). The formation of compounds with higher oxidation states and the degradation of N-containing compounds reduce the conjunction degrees of BrC, diminishing $\pi \rightarrow \pi^*$ electronic transitions and weakening light-absorption capacity.

Table 1 Variations in the signal-intensity-weighted average elemental compositions, molecular weights, O/C ratios, and N/C ratios of different types of BrC before and after photobleaching

aq-BrC	elemental composition	molecular weight	O/C	N/C
before	$C_{8.94}H_{10.22}O_{4.64}N_{1.33}$	210.36	0.52	0.15
after	$C_{8.22}H_{10.17}O_{4.66}N_{1.07}$	198.35	0.57	0.12
p-BrC	elemental composition	molecular weight	O/C	N/C
before	$C_{7.88}H_{8.38}O_{2.47}N_{2.13}S_{0.65}$	193.08	0.31	0.28
after	$C_{7.21}H_{9.17}O_{2.52}N_{1.82}S_{0.68}$	183.25	0.35	0.25
b-BrC	elemental composition	molecular weight	O/C	N/C
before	$C_{15.92}H_{16.68}O_{6.05}N_{1.18}S_{0.31}$	330.96	0.38	0.08
after	$C_{15.42}H_{16.92}O_{6.11}N_{1.07}S_{0.41}$	327.82	0.40	0.07

Figure S6 shows the differential HRMS spectra, the negative peaks represent species consumed after photobleaching. The photooxidation of MG and imidazole-2-carboxaldehyde (2-IC) oligomers (Aiona et al., 2017) with formula $C_{3n}H_{4n}N_2O_{2n-3}$ (n = 2-5; including *m/z* 123.06, 195.08, 267.10, and 339.12), phenols and nitrophenols (Hems and Abbatt, 2018; Magalhães et al., 2017) (including *m/z* 109.03, 138.02, 152.03, 168.03, 182.01, and 183.00), and lignin derivatives (Fleming et al., 2020) (including *m/z* 137.02, 163.04, 245.08, 283.06, and 313.07) were identified as the dominant reactions in the photobleaching of aq-BrC, p-BrC, and b-BrC,

https://doi.org/10.5194/egusphere-2025-5502
Preprint. Discussion started: 20 November 2025

respectively. Compounds identified as products after photobleaching for aq-BrC, p-BrC, and b-BrC are respectively summarized in Tables S4-S6.

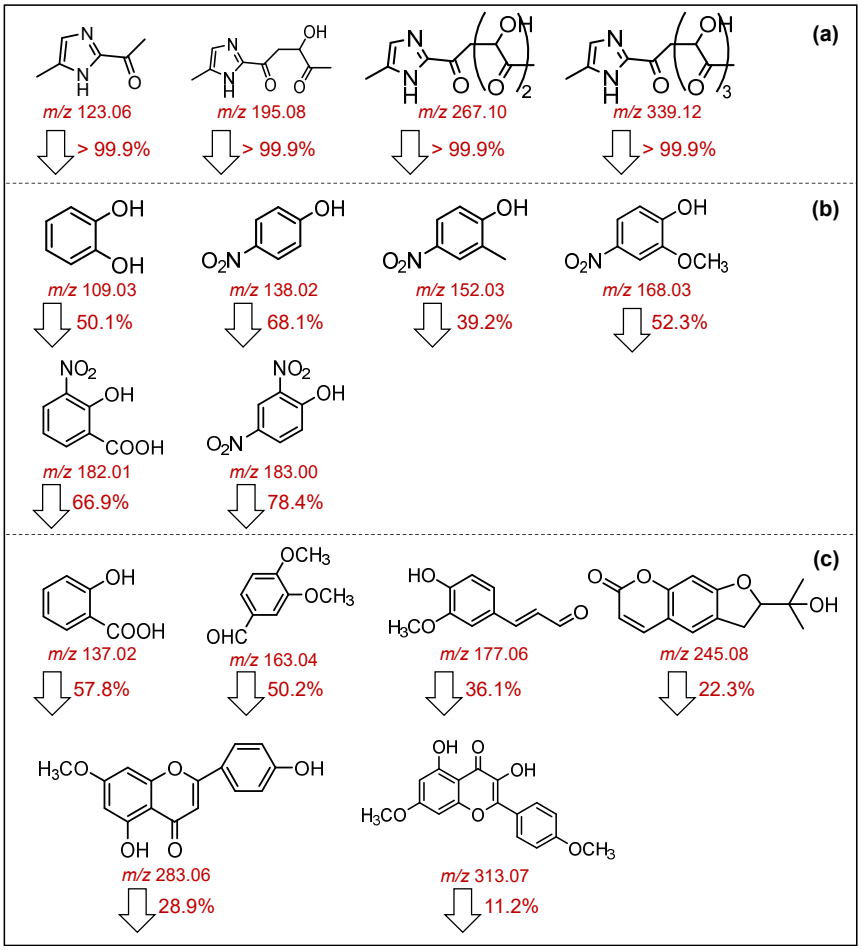

Figure 3 The chemical structures of (a) MG and 2-IC oligomers detected in aq-BrC; (b) phenols and nitrophenols detected in p-BrC, and (c) lignin derivatives detected in b-BrC. The detected *m/z* for these compounds are marked under their structures. The ratios of decline in signal intensities for these compounds after 16 hours of radiation are indicated next to the bottom arrows.

Figure 3 displays the chemical structures of these MG and 2-IC oligomers, phenols and nitrophenols, and lignin derivatives, as well as the declines in their signal intensities after 16 hours of radiation. Variations in HRMS signal intensities represent the changes in the mass concentrations, though specific mass concentrations cannot be derived. Figure 3(a) illustrates the predominant molecular species and the corresponding decline in

https://doi.org/10.5194/egusphere-2025-5502
Preprint. Discussion started: 20 November 2025

MG and 2-IC oligomers during the photobleaching of aq-BrC. Following photobleaching, these oligomers became undetectable (signal-to-noise ratio < 3), experiencing a reduction in signal intensity of >99.9% (Figure 3(a)). This observation is consistent with the nearly complete bleaching of aq-BrC. The high reactivity of the chain structures of MG and 2-IC oligomers with OH radicals (Aiona et al., 2017) explains the elevated k_{BrC} value observed for aq-BrC.

As shown in Figure 3(b), a greater number of electron-withdrawing substituents on the benzene ring correlates with a more significant decline of signal intensity after photobleaching. For instance, 2-methyl-4-nitrophenol (*m/z* 152.03), which bears an electron-donating methyl group in addition to the electron-withdrawing nitro substituent present in 4-nitrophenol (*m/z* 138.02), demonstrates a comparatively lower signal attenuation of 39.2% after photobleaching, whereas 4-nitrophenol exhibits a signal decrease of 68.1%. The electron-withdrawing substituents exert both inductive and resonance effects, effectively diminishing the electron density of the π-system of the aromatic ring. This electron-deficient state enhances the susceptibility of these species to nucleophilic attack by OH radicals, thereby facilitating their photooxidation and contributing to the observed photobleaching behavior. However, the reactivity of these species remains lower than that of MG and 2-IC oligomers, which explains lower k_{BrC} for p-BrC compares to aq-BrC.

In comparison, the signal intensities of the majority of lignin derivatives only decreased by below 50%, corresponding to the lowest k_{BrC} for b-BrC (Figure 3(c)). Specifically, nodakenetin and flavonoids (*m/z* 245.08, 283.06, and 313.07) exhibit highly stabilized molecular structures, wherein the aromatic rings conjugated with oxygen-containing heterocyclic moieties significantly reduce their chemical reactivity, resulting in low k_{BrC} for b-BrC. The chemical stability of lignin derivatives has been also proved by previous laboratory experiment (Wong et al., 2019).

4. Conclusion and Atmospheric Implication

This work demonstrates that BrC exhibits source-dependent photobleaching rates. Specifically, aq-BrC shows the highest k_{BrC}, followed by p-BrC and b-BrC, indicating that light-absorption capacity of b-BrC keep stable during photobleaching. In addition, considering the overwhelming contribution of $k_{BrC,OH}$ to k_{BrC}, the OH oxidation is determined as the predominate pathway of BrC photobleaching. The OH oxidation leads to the formation of compounds with higher oxidation state and lower molecular weights, which decreases the conjunction degree of BrC and therefore results in photobleaching. The oxidation of MG and 2-IC oligomers, phenols and nitrophenols, and lignin derivatives dominate the photobleaching of aq-BrC, p-BrC, and b-BrC, respectively.

Source-dependent k_{BrC} values necessitate explicit consideration of source variability when evaluating BrC's climate effect. Current models often assume constant k_{BrC} based on simplified representative compounds or field data (Hems and Abbatt, 2018; Schnitzler et al., 2022; Wang et al., 2018), yet substantial discrepancies exist. For instance, the reported k_{BrC} values differ by approximately an order of magnitude between field observations and laboratory simulations (Schnitzler et al., 2022; Wang et al., 2018). Spatiotemporal heterogeneity in BrC sources (Xiong et al., 2022) (fossil fuel/biomass combustion, secondary formation) drives global regional variations in k_{BrC}. To further reduce the uncertainties in assessing BrC's global DRE, it is imperative to systematically quantify

https://doi.org/10.5194/egusphere-2025-5502
Preprint. Discussion started: 20 November 2025

the impact of BrC's source and integrate source-dependent data into regional and global climate models.

In addition, the low k_{BrC} for b-BrC explains unexpectedly high BrC absorption in remote regions (e.g., the Arctic). Field data confirm biomass burning contributes 57% of Arctic BrC while < 10% for secondary BrC (Yue et al., 2022). Previous studies have confirmed that biomass burning aerosols contains substantial amounts of lignin derivatives (Wong et al., 2019), which exhibit strong light-absorbing properties and chemical stability in OH oxidation. Therefore, during the long-range transport (Zhang et al., 2025), b-BrC is expected to retain strong absorption, leading to enhancement of the aerosol DRE over large spatial scales. On a global scale, one major source of b-BrC is wildfire events (Wang et al., 2025; Shen et al., 2024; Bond et al., 2004). With the increasing frequency of wildfires (Yue et al., 2013; Hurteau et al., 2014; Cunningham et al., 2024; Jain et al., 2022), the emission of b-BrC is expected to rise correspondingly. In all, b-BrC would exert a significant influence on BrC's global radiative effect.

Associate Content

Code and Data Availability

The data used in this study is available upon request from the corresponding author (zhijunwu@pku.edu.cn).

Author Contributions

Y.Q. and Z.W. designed this work. Y.Q., T.Q., Y.G., and D.L. collected and analyzed the measurement data. Y.Q., T.Q., Y.L, and R.M. analyzed UHPLC-MS data. Z.W. and M.H. edited the manuscript. All authors have read and agreed to submit this manuscript.

Funding

This work is funded by National Natural Science Foundation of China – Youth Program (42507137), China Postdoctoral Science Foundation (2025M771267), and the National Key Research and Development Program of China (2022YFC3701000, Task 4).

Competing Interests

The authors declare that they have no conflict of interest.

Acknowledgements

This research has been supported by the National Natural Science Foundation of China (grant no. 42507137), Chinese Postdoctoral Science Foundation (grant no. 2025M771267), the National Key Research and Development Program of China (grant no. 2022YFC3701000, Task 4).

https://doi.org/10.5194/egusphere-2025-5502
Preprint. Discussion started: 20 November 2025

References

Aiona, P. K., Lee, H. J., Leslie, R., Lin, P., Laskin, A., Laskin, J., Nizkorodov, S. A.: Photochemistry of Products of the Aqueous Reaction of Methylglyoxal with Ammonium Sulfate. ACS Earth and Space Chemistry. 1, 522-532. 10.1021/acsearthspacechem.7b00075, 2017.

Bond, T. C.: Spectral dependence of visible light absorption by carbonaceous particles emitted from coal combustion. Geophysical Research Letters. 28, 4075-4078. https://doi.org/10.1029/2001GL013652, 2001.

Bond, T. C., Streets, D. G., Yarber, K. F., Nelson, S. M., Woo, J.-H., Klimont, Z.: A technology-based global inventory of black and organic carbon emissions from combustion. Journal of Geophysical Research: Atmospheres. 109. https://doi.org/10.1029/2003JD003697, 2004.

Borduas-Dedekind, N., Ossola, R., David, R. O., Boynton, L. S., Weichlinger, V., Kanji, Z. A., McNeill, K.: Photomineralization mechanism changes the ability of dissolved organic matter to activate cloud droplets and to nucleate ice crystals. Atmospheric Chemistry and Physics. 19, 12397-12412. 10.5194/acp-19-12397-2019, 2019.

Brown, H., Liu, X., Pokhrel, R., Murphy, S., Lu, Z., Saleh, R., Mielonen, T., Kokkola, H., Bergman, T., Myhre, G., Skeie, R. B., Watson-Paris, D., Stier, P., Johnson, B., Bellouin, N., Schulz, M., Vakkari, V., Beukes, J. P., van Zyl, P. G., Liu, S., Chand, D.: Biomass burning aerosols in most climate models are too absorbing. Nature Communications. 12, 277. 10.1038/s41467-020-20482-9, 2021.

Chen, L.-W. A., Chow, J. C., Wang, X., Cao, J., Mao, J., Watson, J. G.: Brownness of Organic Aerosol over the United States: Evidence for Seasonal Biomass Burning and Photobleaching Effects. Environmental Science & Technology. 55, 8561-8572. 10.1021/acs.est.0c08706, 2021.

Chen, Q., Sun, H., Wang, J., Shan, M., Yang, X., Deng, M., Wang, Y., Zhang, L.: Long-life type — The dominant fraction of EPFRs in combustion sources and ambient fine particles in Xi'an. Atmos. Environ. 219, 117059. https://doi.org/10.1016/j.atmosenv.2019.117059, 2019.

Choudhary, V., Roson, M. L., Guo, X., Gautam, T., Gupta, T., Zhao, R.: Aqueous-phase photochemical oxidation of water-soluble brown carbon aerosols arising from solid biomass fuel burning. Environmental Science: Atmospheres. 3, 816-829. 10.1039/D2EA00151A, 2023.

Chung, C. E., Ramanathan, V., Decremer, D.: Observationally constrained estimates of carbonaceous aerosol radiative forcing. Proceedings of the National Academy of Sciences USA. 109, 11624-11629. 10.1073/pnas.1203707109, 2012.

Corr, C. A., Hall, S. R., Ullmann, K., Anderson, B. E., Beyersdorf, A. J., Thornhill, K. L., Cubison, M. J., Jimenez, J. L., Wisthaler, A., Dibb, J. E.: Spectral absorption of biomass burning aerosol determined from retrieved single scattering albedo during ARCTAS. Atmospheric Chemistry and Physics. 12, 10505-10518. 10.5194/acp-12-10505-2012, 2012.

Cunningham, C. X., Williamson, G. J., Bowman, D. M. J. S.: Increasing frequency and intensity of the most extreme wildfires on Earth. Nature Ecology & Evolution. 8, 1420-1425. 10.1038/s41559-024-02452-2, 2024.

Dalton, A. B., Nizkorodov, S. A.: Photochemical Degradation of 4-Nitrocatechol and 2,4-Dinitrophenol in a Sugar-Glass Secondary Organic Aerosol Surrogate. Environmental Science & Technology. 55, 14586-14594. 10.1021/acs.est.1c04975, 2021.

Dasari, S., Andersson, A., Bikkina, S., Holmstrand, H., Budhavant, K., Satheesh, S., Asmi, E., Kesti, J., Backman, J., Salam, A., Bisht, D. S., Tiwari, S., Hameed, Z., Gustafsson, Ö.: Photochemical degradation affects the light

https://doi.org/10.5194/egusphere-2025-5502
Preprint. Discussion started: 20 November 2025

absorption of water-soluble brown carbon in the South Asian outflow. Science Advances. 5, eaau8066. 10.1126/sciadv.aau8066, 2019.

De Haan, D. O., Hawkins, L. N., Welsh, H. G., Pednekar, R., Casar, J. R., Pennington, E. A., de Loera, A., Jimenez, N. G., Symons, M. A., Zauscher, M., Pajunoja, A., Caponi, L., Cazaunau, M., Formenti, P., Gratien, A., Pangui, E., Doussin, J.-F.: Brown Carbon Production in Ammonium- or Amine-Containing Aerosol Particles by Reactive Uptake of Methylglyoxal and Photolytic Cloud Cycling. Environmental Science & Technology. 51, 7458-7466. 10.1021/acs.est.7b00159, 2017.

Fan, X., Yu, X., Wang, Y., Xiao, X., Li, F., Xie, Y., Wei, S., Song, J., Peng, P. a.: The aging behaviors of chromophoric biomass burning brown carbon during dark aqueous hydroxyl radical oxidation processes in laboratory studies. Atmospheric Environment. 205, 9-18. https://doi.org/10.1016/j.atmosenv.2019.02.039, 2019.

Fleming, L. T., Ali, N. N., Blair, S. L., Roveretto, M., George, C., Nizkorodov, S. A.: Formation of Light-Absorbing Organosulfates during Evaporation of Secondary Organic Material Extracts in the Presence of Sulfuric Acid. ACS Earth and Space Chemistry. 3, 947-957. 10.1021/acsearthspacechem.9b00036, 2019.

Fleming, L. T., Lin, P., Roberts, J. M., Selimovic, V., Yokelson, R., Laskin, J., Laskin, A., Nizkorodov, S. A.: Molecular composition and photochemical lifetimes of brown carbon chromophores in biomass burning organic aerosol. Atmospheric Chemistry and Physics. 20, 1105-1129. 10.5194/acp-20-1105-2020, 2020.

Gao, Y., Zhang, Y.: Optical properties investigation of the reactions between methylglyoxal and glycine/ammonium sulfate. Spectrochimica Acta Part A: Molecular and Biomolecular Spectroscopy. 215, 112-121. https://doi.org/10.1016/j.saa.2019.02.087, 2019.

Heald, C. L., Ridley, D. A., Kroll, J. H., Barrett, S. R. H., Cady-Pereira, K. E., Alvarado, M. J., Holmes, C. D.: Contrasting the direct radiative effect and direct radiative forcing of aerosols. Atmospheric Chemistry and Physics. 14, 5513-5527. 10.5194/acp-14-5513-2014, 2014.

Hems, R. F., Abbatt, J. P. D.: Aqueous Phase Photo-oxidation of Brown Carbon Nitrophenols: Reaction Kinetics, Mechanism, and Evolution of Light Absorption. ACS Earth and Space Chemistry. 2, 225-234. 10.1021/acsearthspacechem.7b00123, 2018.

Hems, R. F., Schnitzler, E. G., Bastawrous, M., Soong, R., Simpson, A. J., Abbatt, J. P. D.: Aqueous Photoreactions of Wood Smoke Brown Carbon. ACS Earth and Space Chemistry. 4, 1149-1160. 10.1021/acsearthspacechem.0c00117, 2020.

Hems, R. F., Schnitzler, E. G., Liu-Kang, C., Cappa, C. D., Abbatt, J. P. D.: Aging of Atmospheric Brown Carbon Aerosol. ACS Earth and Space Chemistry. 5, 722-748. 10.1021/acsearthspacechem.0c00346, 2021.

Hurteau, M. D., Westerling, A. L., Wiedinmyer, C., Bryant, B. P.: Projected Effects of Climate and Development on California Wildfire Emissions through 2100. Environmental Science & Technology. 48, 2298-2304. 10.1021/es4050133, 2014.

Jain, P., Castellanos-Acuna, D., Coogan, S. C. P., Abatzoglou, J. T., Flannigan, M. D.: Observed increases in extreme fire weather driven by atmospheric humidity and temperature. Nature Climate Change. 12, 63-70. 10.1038/s41558-021-01224-1, 2022.

Jo, D. S., Park, R. J., Lee, S., Kim, S. W., Zhang, X.: A global simulation of brown carbon: implications for photochemistry and direct radiative effect. Atmospheric Chemistry and Physics. 16, 3413-3432. 10.5194/acp-16-3413-2016, 2016.

Kirchstetter, T. W., Novakov, T., Hobbs, P. V.: Evidence that the spectral dependence of light absorption by aerosols is affected by organic carbon. Journal of Geophysical Research: Atmospheres. 109.

https://doi.org/10.5194/egusphere-2025-5502
Preprint. Discussion started: 20 November 2025

https://doi.org/10.1029/2004JD004999, 2004.

Li, Y., Fu, T.-M., Yu, J. Z., Zhang, A., Yu, X., Ye, J., Zhu, L., Shen, H., Wang, C., Yang, X., Tao, S., Chen, Q., Li, Y., Li, L., Che, H., Heald, C. L.: Nitrogen dominates global atmospheric organic aerosol absorption. Science. 387, 989-995. 10.1126/science.adr4473, 2025.

Lin, P., Huang, X.-F., He, L.-Y., Zhen Yu, J.: Abundance and size distribution of HULIS in ambient aerosols at a rural site in South China. Journal of Aerosol Science. 41, 74-87. https://doi.org/10.1016/j.jaerosci.2009.09.001, 2010.

Lin, P., Bluvshtein, N., Rudich, Y., Nizkorodov, S. A., Laskin, J., Laskin, A.: Molecular Chemistry of Atmospheric Brown Carbon Inferred from a Nationwide Biomass Burning Event. Environmental Science & Technology. 51, 11561-11570. 10.1021/acs.est.7b02276, 2017.

Liu-Kang, C., Gallimore, P. J., Liu, T., Abbatt, J. P. D.: Photoreaction of biomass burning brown carbon aerosol particles. Environmental Science: Atmospheres. 2, 270-278. 10.1039/d1ea00088h, 2022.

Liu, D., He, C., Schwarz, J. P., Wang, X.: Lifecycle of light-absorbing carbonaceous aerosols in the atmosphere. npj Climate and Atmospheric Science. 3, 40. 10.1038/s41612-020-00145-8, 2020.

Liu, Y., Huang, R.-J., Lin, C., Yuan, W., Li, Y. J., Zhong, H., Yang, L., Wang, T., Huang, W., Xu, W., Huang, D. D., Huang, C.: Nitrate-Photolysis Shortens the Lifetimes of Brown Carbon Tracers from Biomass Burning. Environmental Science & Technology. 59, 640-649. 10.1021/acs.est.4c06123, 2025.

Magalhães, A. C. O., Esteves da Silva, J. C. G., Pinto da Silva, L.: Density Functional Theory Calculation of the Absorption Properties of Brown Carbon Chromophores Generated by Catechol Heterogeneous Ozonolysis. ACS Earth and Space Chemistry. 1, 353-360. 10.1021/acsearthspacechem.7b00061, 2017.

Müller, S., Giorio, C., Borduas-Dedekind, N.: Tracking the Photomineralization Mechanism in Irradiated Lab-Generated and Field-Collected Brown Carbon Samples and Its Effect on Cloud Condensation Nuclei Abilities. ACS Environmental Au. 3, 164-178. 10.1021/acsenvironau.2c00055, 2023.

Qiu, Y., Qiu, T., Wu, Z., Liu, Y., Fang, W., Man, R., Liu, Y., Wang, J., Meng, X., Chen, J., Liang, D., Guo, S., Hu, M.: Observational Evidence of Brown Carbon Photobleaching in Urban Atmosphere at Molecular Level. Environmental Science and Technology Letters. 11, 1032-1039. 10.1021/acs.estlett.4c00647, 2024.

Saleh, R., Marks, M., Heo, J., Adams, P. J., Donahue, N. M., Robinson, A. L.: Contribution of brown carbon and lensing to the direct radiative effect of carbonaceous aerosols from biomass and biofuel burning emissions. Journal of Geophysical Research: Atmospheres. 120, 10,285-210,296. https://doi.org/10.1002/2015JD023697, 2015.

Saleh, R.: From Measurements to Models: Toward Accurate Representation of Brown Carbon in Climate Calculations. Current Pollution Reports. 6, 90-104. 10.1007/s40726-020-00139-3, 2020.

Schnitzler, E. G., Abbatt, J. P. D.: Heterogeneous OH oxidation of secondary brown carbon aerosol. Atmospheric Chemistry and Physics. 18, 14539-14553. 10.5194/acp-18-14539-2018, 2018.

Schnitzler, E. G., Gerrebos, N. G. A., Carter, T. S., Huang, Y., Heald, C. L., Bertram, A. K., Abbatt, J. P. D.: Rate of atmospheric brown carbon whitening governed by environmental conditions. Proceedings of the National Academy of Sciences. 119, e2205610119. 10.1073/pnas.2205610119, 2022.

Shan, M., Carter, E., Baumgartner, J., Deng, M., Clark, S., Schauer, J. J., Ezzati, M., Li, J., Fu, Y., Yang, X.: A user-centered, iterative engineering approach for advanced biomass cookstove design and development. Environ. Res. Lett. 12, 095009. 10.1088/1748-9326/aa804f, 2017.

Shen, Y., Pokhrel, R. P., Sullivan, A. P., Levin, E. J. T., Garofalo, L. A., Farmer, D. K., Permar, W., Hu, L., Toohey, D. W., Campos, T., Fischer, E. V., Murphy, S. M.: Understanding the mechanism and importance of brown carbon

https://doi.org/10.5194/egusphere-2025-5502
Preprint. Discussion started: 20 November 2025

bleaching across the visible spectrum in biomass burning plumes from the WE-CAN campaign. Atmospheric Chemistry and Physics. 24, 12881-12901. 10.5194/acp-24-12881-2024, 2024.

Wang, Q., Zhou, Y., Ma, N., Zhu, Y., Zhao, X., Zhu, S., Tao, J., Hong, J., Wu, W., Cheng, Y., Su, H.: Review of Brown Carbon Aerosols in China: Pollution Level, Optical Properties, and Emissions. Journal of Geophysical Research: Atmospheres. 127, e2021JD035473. https://doi.org/10.1029/2021JD035473, 2022.

Wang, X., Heald, C. L., Ridley, D. A., Schwarz, J. P., Spackman, J. R., Perring, A. E., Coe, H., Liu, D., Clarke, A. D.: Exploiting simultaneous observational constraints on mass and absorption to estimate the global direct radiative forcing of black carbon and brown carbon. Atmospheric Chemistry and Physics. 14, 10989-11010. 10.5194/acp-14-10989-2014, 2014.

Wang, X., Heald, C. L., Liu, J., Weber, R. J., Campuzano-Jost, P., Jimenez, J. L., Schwarz, J. P., Perring, A. E.: Exploring the observational constraints on the simulation of brown carbon. Atmospheric Chemistry and Physics. 18, 635-653. 10.5194/acp-18-635-2018, 2018.

Wang, X., Chakrabarty, R. K., Schwarz, J. P., Murphy, S. M., Levin, E. J. T., Howell, S. G., Guo, H., Campuzano-Jost, P., Jimenez, J. L.: Dark brown carbon from biomass burning contributes to significant global-scale positive forcing. One Earth. 8, 101205. https://doi.org/10.1016/j.oneear.2025.101205, 2025.

Wang, Y., Hu, M., Lin, P., Guo, Q., Wu, Z., Li, M., Zeng, L., Song, Y., Zeng, L., Wu, Y., Guo, S., Huang, X., He, L.: Molecular Characterization of Nitrogen-Containing Organic Compounds in Humic-like Substances Emitted from Straw Residue Burning. Environmental Science & Technology. 51, 5951-5961. 10.1021/acs.est.7b00248, 2017.

Wang, Y., Hu, M., Lin, P., Tan, T., Li, M., Xu, N., Zheng, J., Du, Z., Qin, Y., Wu, Y., Lu, S., Song, Y., Wu, Z., Guo, S., Zeng, L., Huang, X., He, L.: Enhancement in Particulate Organic Nitrogen and Light Absorption of Humic-Like Substances over Tibetan Plateau Due to Long-Range Transported Biomass Burning Emissions. Environmental Science & Technology. 53, 14222-14232. 10.1021/acs.est.9b06152, 2019.

Wong, J. P. S., Tsagkaraki, M., Tsiodra, I., Mihalopoulos, N., Violaki, K., Kanakidou, M., Sciare, J., Nenes, A., Weber, R. J.: Atmospheric evolution of molecular-weight-separated brown carbon from biomass burning. Atmospheric Chemistry and Physics. 19, 7319-7334. 10.5194/acp-19-7319-2019, 2019.

Xiong, R., Li, J., Zhang, Y., Zhang, L., Jiang, K., Zheng, H., Kong, S., Shen, H., Cheng, H., Shen, G., Tao, S.: Global brown carbon emissions from combustion sources. Environmental Science and Ecotechnology. 12, 100201. https://doi.org/10.1016/j.ese.2022.100201, 2022.

Xu, L., Lin, G., Liu, X., Wu, C., Wu, Y., Lou, S.: Constraining Light Absorption of Brown Carbon in China and Implications for Aerosol Direct Radiative Effect. Geophysical Research Letters. 51, e2024GL109861. https://doi.org/10.1029/2024GL109861, 2024.

Yang, L., Huang, R.-J., Yuan, W., Huang, D. D., Huang, C.: pH-Dependent Aqueous-Phase Brown Carbon Formation: Rate Constants and Implications for Solar Absorption and Atmospheric Photochemistry. Environmental Science & Technology, 1236-1243. 10.1021/acs.est.3c07631, 2024.

Yue, S., Zhu, J., Chen, S., Xie, Q., Li, W., Li, L., Ren, H., Su, S., Li, P., Ma, H., Fan, Y., Cheng, B., Wu, L., Deng, J., Hu, W., Ren, L., Wei, L., Zhao, W., Tian, Y., Pan, X., Sun, Y., Wang, Z., Wu, F., Liu, C.-Q., Su, H., Penner, J. E., Pöschl, U., Andreae, M. O., Cheng, Y., Fu, P.: Brown carbon from biomass burning imposes strong circum-Arctic warming. One Earth. 5, 293-304. https://doi.org/10.1016/j.oneear.2022.02.006, 2022.

Yue, X., Mickley, L. J., Logan, J. A., Kaplan, J. O.: Ensemble projections of wildfire activity and carbonaceous aerosol concentrations over the western United States in the mid-21st century. Atmospheric Environment. 77, 767-780. https://doi.org/10.1016/j.atmosenv.2013.06.003, 2013.

https://doi.org/10.5194/egusphere-2025-5502
Preprint. Discussion started: 20 November 2025

Zeng, L., Zhang, A., Wang, Y., Wagner, N. L., Katich, J. M., Schwarz, J. P., Schill, G. P., Brock, C., Froyd, K. D., Murphy, D. M., Williamson, C. J., Kupc, A., Scheuer, E., Dibb, J., Weber, R. J.: Global Measurements of Brown Carbon and Estimated Direct Radiative Effects. Geophysical Research Letters. 47, e2020GL088747. https://doi.org/10.1029/2020GL088747, 2020.

Zeng, Y., Ning, Y., Shen, Z., Zhang, L., Zhang, T., Lei, Y., Zhang, Q., Li, G., Xu, H., Ho, S. S. H., Cao, J.: The Roles of N, S, and O in Molecular Absorption Features of Brown Carbon in PM2.5 in a Typical Semi-Arid Megacity in Northwestern China. Journal of Geophysical Research: Atmospheres. 126, e2021JD034791. https://doi.org/10.1029/2021JD034791, 2021.

Zhang, Q., Wang, Y., Xiao, Q., Geng, G., Davis, S. J., Liu, X., Yang, J., Liu, J., Huang, W., He, C., Luo, B., Martin, R. V., Brauer, M., Randerson, J. T., He, K.: Long-range PM2.5 pollution and health impacts from the 2023 Canadian wildfires. Nature. 10.1038/s41586-025-09482-1, 2025.

Zhang, X., Chen, S., Kang, L., Yuan, T., Luo, Y., Alam, K., Li, J., He, Y., Bi, H., Zhao, D.: Direct Radiative Forcing Induced by Light-Absorbing Aerosols in Different Climate Regions Over East Asia. Journal of Geophysical Research: Atmospheres. 125, e2019JD032228. https://doi.org/10.1029/2019JD032228, 2020.